Water Science & Technology

IWA PUBLISHING

Water Science & Technology Vol 85 No 10, 2797 doi: 10.2166/wst.2022.152

$Fe@Fe_2O_3$-loaded biochar as an efficient heterogeneous Fenton catalyst for organic pollutants removal

Diwei Chen, Zhiyan Zheng, Feiji Zhang, Rufu Ke, Nan Sun, Yonghao Wang* and Yongjing Wang

Fujian Provincial Engineering Research Center for High-value Utilization Technology of Plant Resources, College of Environment and Safety Engineering, Fuzhou University, Fuzhou, Fujian, 350108, P. R. China
*Corresponding author. E-mail: wangyh@fzu.edu.cn

ABSTRACT

With increased demand for various chemical raw materials, sudden pollution incidents are more prone to occur during their transportation and usage, threatening the environment and human health. In this study, discarded tea stalks were recycled into composite materials (FSC-X00: X represents the calcination temperature) by impregnating tea stalks in Fe^{2+} solution combined with subsequent calcination. X-ray diffractometer (XRD) and X-ray photoelectron spectroscopy (XPS) patterns verified the existence of Fe^0 and Fe_2O_3, and Fe_2O_3 was gradually reduced to Fe^0 when the calcination temperature was raised from 700 °C to 900 °C. FSC-X00 was adopted as a heterogeneous catalyst for activating H_2O_2 to quickly degrade phenol in the water system. The degradation experiments indicated that FSC-600 exhibited superior degradation performance for phenol (20 mg/L) within 5 min and 80% total organic carbon (TOC) removal rate at pH = 3 within 30 min. The effects of the calcination temperature, the pH value and the amount of H_2O_2 on the degradation efficiency were investigated. Competing experiments showed that fulvic acid (FA) and inorganic salts Na^+ had little effect on the degradation performance. The FSC-600 catalyst can be reused by thermal reduction. In addition, it was found that FSC-600 has a good degradation effect on ciprofloxacin (CIP), norfloxacin (NOR) and enrofloxacin (ENR), indicating that FSC-600 catalysts are a promising candidate for quick degradation of organic pollutants by Fenton reaction. Electron paramagnetic resonance (EPR) spectra analysis indicated that •OH is the dominant reactive oxygen species (ROS) and part $^1O_2$ from O_2 also participated in the degradation. This study provides an example of creating catalysts from organic solid waste for use in emergency treatment for phenol.

Key words: biochar, heterogeneous Fenton, organic pollutants, wastewater treatment

HIGHLIGHTS

- $Fe@Fe_2O_3$-loaded biochar (FSC-600) was prepared by waste tea stalks and $FeSO_4$ combined with calcinations.
- FSC-600-H_2O_2 exhibited superior degradation performance for phenol, ciprofloxacin, norfloxacin and enrofloxacin in a short period.
- Mechanism analysis indicates that •OH is the dominant ROS and a little $^1O_2$ from O_2 also participated the degradation.

GRAPHICAL ABSTRACT

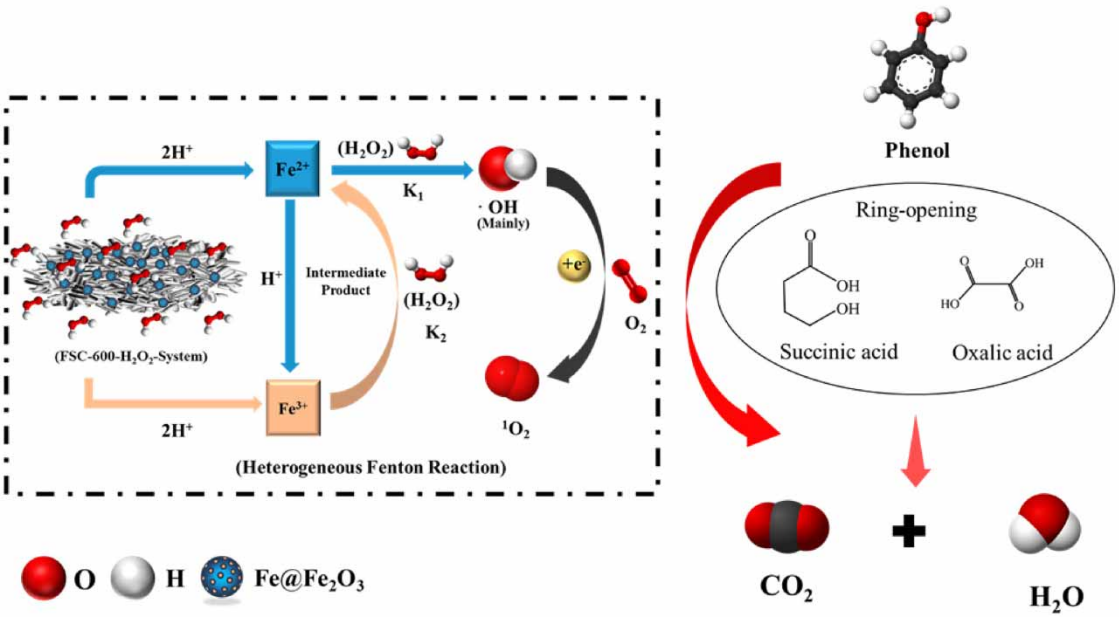

1. INTRODUCTION

Various organic pollutants, such as aromatic pollutants, are often detected in wastewater effluents of pharmaceutical manufacturers and surface water. Aromatic pollutants are resistant to biodegradation or other methods, because of the stable benzene ring structure. In addition, the toxicity of aromatic pollutants can cause serious harm to the environment and human health (Ye *et al.* 2020). In recent years, demand for all forms of chemical raw materials has increased with economic development. As a result, sudden water pollution incidents are likely to occur more frequently. For example, phenol leakage occurred in 2020 in Guangdong Province, China and the leaked phenol flowed into the Rong River, resulting in extremely serious environmental pollution. Incidents like this are often characterized by high concentration and large scale, and reducing their harmfulness to the minimum range efficiently without new environmental pollutants is challenging.

Advanced oxidation processes (AOP_S) have been regarded as an efficient method to remove organic pollutants from wastewater (Bilińska & Gmurek 2021; Rayaroth *et al.* 2021; Lin *et al.* 2022; Yuan *et al.* 2022), including traditional Fenton oxidation, electrochemical oxidation (Yang *et al.* 2021), ozonation (Xu *et al.* 2022), photochemical oxidation (Kilic *et al.* 2019) and microwave oxidation (Adekunle *et al.* 2021), etc. Fenton oxidation is better-suited to deal with sudden environmental water pollution incidents compared with other AOPs, because other AOPs involve complex operation and time-consuming, special devices. Therein, persulfate oxidation has received more attention because of its excellent catalytic performance (Su *et al.* 2020; Zhang *et al.* 2022). However, the Fenton reaction is an efficient method to deal with sudden water pollution events as there is no secondary pollution (Xiaoliang *et al.* 2021).

At present, the most commonly used homogeneous Fenton method has the disadvantage of producing a large amount of iron sludge and narrow pH ranges (Wang *et al.* 2016). Therefore, many studies have focused on the heterogeneous catalyst to alleviate the formation of iron sludge (Xu & Wang 2011; Zha *et al.* 2014). Among numerous heterogeneous catalysts, Fe and its oxides nanoparticles have received more attention due to its abundant reserves and excellent catalytic performance. However, nanoparticles can gradually agglomerate during the application process, resulting in a sharp reduction in the ability to activate H_2O_2. Hence, a suitable matrix is often adopted to effectively load the metal or its oxide, so as to improve the ability to activate H_2O_2 (Pan *et al.* 2021). However, the reaction time for heterogeneous Fenton reaction based on Fe or its oxide is generally about 20–60 min. Sudden water pollution events require rapid and effective treatment, so finding a cost-effective and efficient heterogeneous Fenton catalyst to treat these events is of great importance.

Biochar is often used as a matrix of various composite materials because of its abundant pores and large specific surface area (Liang *et al.* 2021; Qi *et al.* 2022). In this study, the discarded tea stalks were recycled into composites materials by iron

divalent solution dipping and subsequent calcination, using a heterogeneous Fenton catalyst to quickly treat phenol pollution. This study will explore new possibilities of using organic solid waste to synthesise composite materials to treat wastewater.

2. EXPERIMENTS

2.1. Materials and chemicals

Ferrous sulfate ($FeSO_4{\cdot}7H_2O$, 99%), sodium borohydride ($NaBH_4$, 98%), sulfuric acid (H_2SO_4, 98%), sodium hydroxide (NaOH, 96%), anhydrous ethanol (C_2H_6O, 99%), phenol (C_6H_5OH, 99%), ciprofloxacin ($C_{17}H_{18}FN_3O_3$, 98%), enrofloxacin ($C_{19}H_{22}FN_3$-O, 98%), norfloxacin ($C_{16}H_{18}FN_3O_3$, 98%), bisphenol A ($C_{15}H_{16}O_2$, 99.99%) and methanol (CH_4O, 99.99%) were purchased from Sinopharmaceutical Chemical Reagent (China) Co., Ltd. Hydrogen peroxide (H_2O_2, AR, 30%), benzoic acid ($C_7H_6O_2$, 99%), ammonium ferrous sulfate ($Fe(NH_4)_2(SO_4)_26H_2O$, 99%), hydroxylamine hydrochloride (NH_3OHCl, 99%), 1meme 10-phenanthroline (anhydrous) ($C_{12}H_8N_2$, 99%), and tert-butanol ($C_4H_{10}O$, 99%) were purchased from China Aladdin Chemical Co., Ltd. All reagents were used directly without further purification, and the aqueous solutions involved in the experiment were all prepared with ultra-pure water.

2.2. Catalyst synthesis

Biochar was produced by the pyrolysis of tea stalk waste (sourced from FuJian Province, China). First, the collected solid was washed with ultra-pure water three times to remove surface dirt, and then dried in an oven at 60 °C. Then, the dried tea stalk waste was crushed and sieved (60-mesh sieve) into powder, which was pyrolyzed for 4 h at 600 °C (heating rate 5 °C/min) under Ar (purity 99%) atmosphere. The biochar collected was named BC.

1 g of biochar (BC) was dispersed in 50 mL of Fe^{2+} solution (0.28 mol/L), and the suspension was placed on a shaker operated at 200 rpm for 8 h. The precipitate was collected by centrifugal separation and washed with ultra-pure water and ethanol three times. The solid obtained was dispersed in 100 mL of ultra-pure water, with 40 mL of sodium borohydride (0.08 mol/L) slowly dripped in, then followed by reaction for 1 h. Finally, the black precipitate was washed with ultra-pure water and ethanol three times and dried in the oven at 60 °C (named precursor). The powders were calcined under Ar (purity 99%) atmosphere at various temperatures (600, 700, 800 and 900 °C) at a heating rate of 5 °C/min, and kept for 1 h. The sample obtained was recorded as FSC-X00 (X is the calcination temperature), and was stored in a vacuum dryer for later experiments.

2.3. Characterizations

The crystal structure information of FSC-X00 was obtained by X-ray diffractometer (XRD, Rigaku MiniFlex 600, Japan). The morphology and structure of FSC-600 were observed by scanning electron microscope (SEM, FEI QUANTA 250, USA). The functional group information of FSC-X00 was collected by Fourier transform infrared spectroscopy (FT-IR, Thermo Scientific Nicolet iS10, USA). The composition and chemical structure of FSC-600 were analyzed by Thermo Fisher Scientific K-Alpha X-ray spectroscopy (XPS, Thermo Scientific ESCALAB 250Xi, USA). The binding energies of all elements were calibrated with reference to C1 s (284.8 eV).

2.4. Degradation experiments

All experiments, unless otherwise specified, were conducted in a 100 mL glass flask in a constant temperature shaker (25 °C). Typically, a 20 mg catalyst was first dispersed into 50 mL of phenol aqueous solution (20 mg/L). Solution pH was adjusted to 3, 4, 6, 8 with NaOH (1 mol/L) or H_2SO_4 (1 mol/L) solution.

The concentration of phenol was tested by UV-vis spectrophotometry. The concentrations of CIP, ENR, NOR and BPA were analyzed by High Performance Liquid Chromatography (HPLC, Agilent 1200, USA). The separation of degradation products was conducted by Agilent Eclipse XDB-C18 column (5 μm × 4.6 mm × 250 mm). Mobile phase A was methanol, mobile phase B was 0.1% formic acid and water mixed solution (70 : 30 v/v), the flow rate was 0.5 mL/min, the injection volume was 20 μL, and the detection wavelengths were 279 nm (CIP (Normile *et al.* 2017)), 290 nm (BPA (Yang *et al.* 2018; Zhang *et al.* 2021)), 278 nm (ENR (Dror *et al.* 2020; Xiao *et al.* 2020)) and 276 nm (NOR (Chen *et al.* 2021; Mohan *et al.* 2021)). Samples were collected at 30 min, 60 min, 120 min, 240 min, 480 min and a total organic carbon analyzer (TOC, Analytik Jena AG, Germany) was used to assess the changes in organic carbon.

The concentrations of Fe^{2+} and total irons were measured by a 1,10-phenanthroline method. Samples were analyzed by measuring the characteristic absorption peak of Fe^{2+}-1,10-phenanthroline complex at 510 nm with a UV–vis spectrophotometer. Hydroxylamine hydrochloride was used as the reducing agent for the total iron concentration measurement.

Different dosages of H_2O_2 (2 mmol/L, 4 mmol/L, 8 mmol/L, 20 mmol/L) and different dosages of FSC-X00 (0.1 g/L, 0.2 g/L, 0.3 g/L, 0.4 g/L) were added into the phenol solution and stirred. To compare the role of BC, FSC-X00, H_2O_2 during the degradation process, five groups of experiments (BC, BC/H_2O_2, H_2O_2, FSC-X00, FSC-X00-H_2O_2) were conducted. After washing and drying, the used FSC-600 was tested for cycle stability and reactivated by high-temperature calcination named FSC-600H.

At each interval (0.5, 1, 2, 5, 10, 15, 30, 40 min), 2 mL of solution was removed from the reactor, and filtered by a 0.22 μm pore film to measure the concentration of phenol. All the above experiments were repeated three times.

3. RESULTS AND DISCUSSION

3.1. Characterization

Figure 1(a) and 1(b) show the XRD patterns and FTIR spectra of FSC-X00 materials. As seen in Figure 1(a), the diffraction peak at 35.4 °, 45.1 ° and 65.02 ° can be attributed to the (311), (110) and (200) crystal plane of Fe_2O_3 (PDF#73-0603). The peaks locating at 45.1 ° and 65.02 ° are attributed to Fe^0 (PDF#87-0721). But the peak at 26.2 ° attributed to biochar (PDF#75-0444, Figure S1a) is invisible because the peak intensity of Fe_2O_3 and Fe^0 outperform that of biochar. In addition, the intensity of the diffraction peak of Fe^0 increases with the increase of calcination temperature. However, the peak intensity of Fe_2O_3 increases first and then decreases with the increase of calcination temperature. When the calcination temperature is 900 °C, the diffraction peak of Fe_2O_3 disappears. We think that Fe_2O_3 particles underwent grain growth before 700 °C and Fe_2O_3 was reduced to Fe^0 by biochar after 700 °C, which is consistent with previous research (Dong *et al.* 2016). From Figure 2(b), we can see that the Fe-O stretching vibration band belonging to Fe_2O_3 at 681 cm^{-1} gradually disappears when the temperature increases from 600 °C to 900 °C, which is consistent with the XRD analysis. Li *et al.* (Li *et al.* 2020) found a similar experimental phenomenon. Figure S1b shows that the peak of precursor at 1,105 cm^{-1} can be attributed to the stretching vibration band in C-OH, and its band shifts to 1,232 cm^{-1} after calcination, which may be due to the transformation of C-OH to C-O-C during calcination. The peak gradually disappears when the calcination temperature continues to rise at 800 °C, which may be due to bond-breaking as temperature rises (Liu *et al.* 2010).

Figure 2 displays the SEM images of biochar BC-600 and FSC-600. As shown in Figure 2(a) and Figure S2a, the biochar exhibits abundant honeycomb-like macropores and the BET specific surface areas (SSA) and average pore size (APS) of BC were 149 m^2/g and 11.69 nm (Table S1), respectively, which are beneficial for the flow of solution, enabling the loading of Fe^{2+}. In addition, the surface negative charge promoted the adsorption of Fe^{2+} (Figure S2b), ensuring the formation of Fe

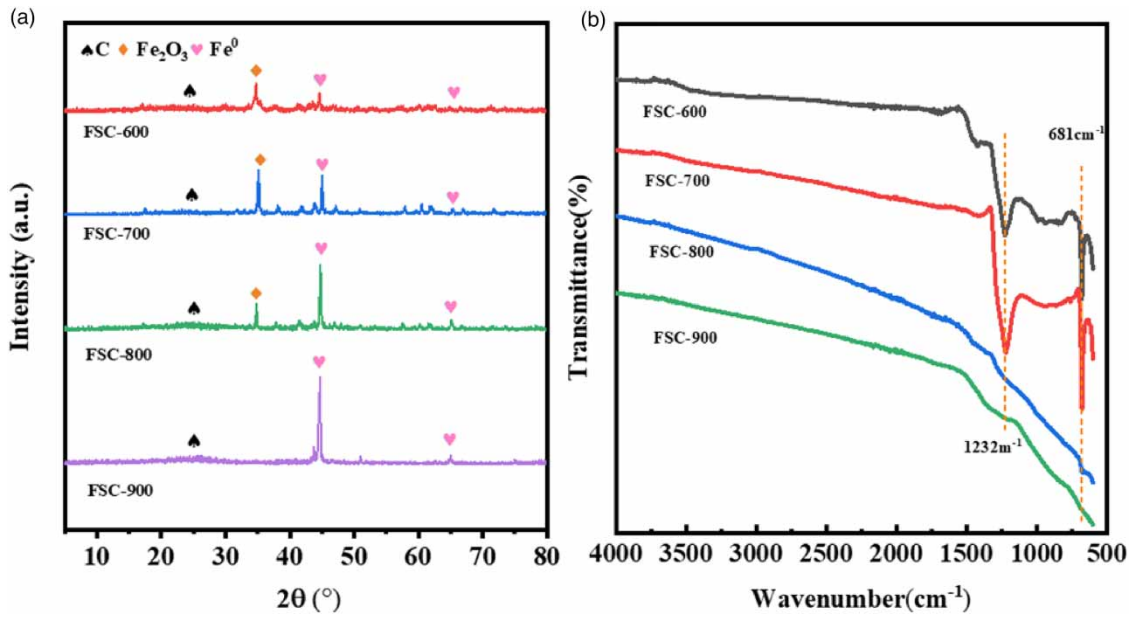

Figure 1 | (a) XRD pattern of FSC-X00; (b) FTIR spectra of FSC-X00.

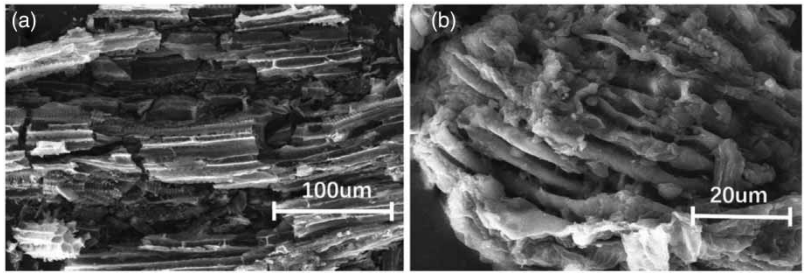

Figure 2 | The SEM images of (a) BC and (b) FSC-600.

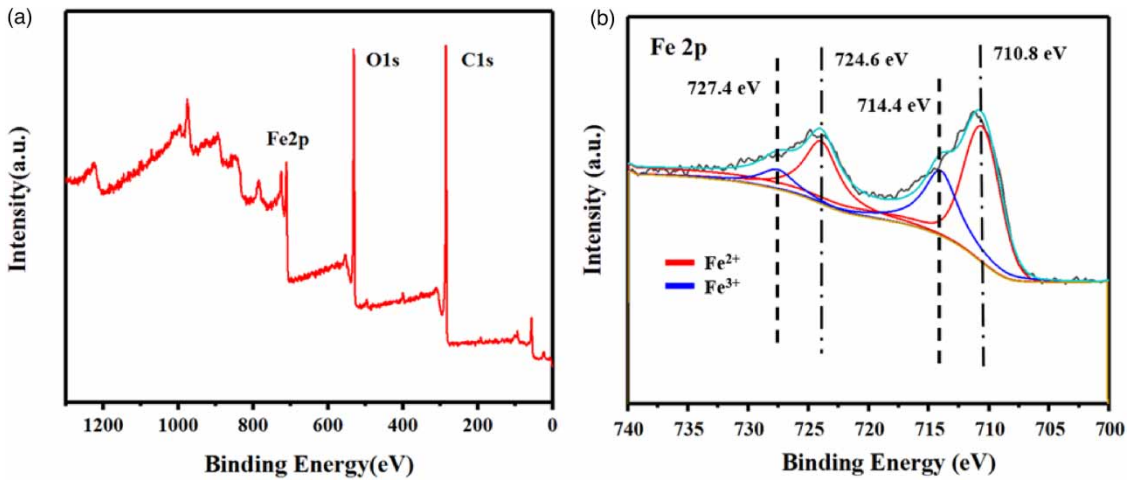

Figure 3 | (a) XPS survey spectra of FSC-600; (b) XPS spectra of Fe 2p.

or Fe_2O_3. As shown in Figure 2(b), the tubular pores were filled with a large number of particles after calcination, which can be attributed to Fe and Fe_2O_3 according to XRD data.

Figure 3 shows XPS spectra of FSC-600. Figure 3(a) shows that the peak at 710, 532, and 284 eV correspond to Fe 2p, O 1 s, and C 1 s, respectively. This proves that the catalyst was composed of Fe, O and C element. Figure 3(b) shows the Fe 2p high-resolution spectra of FSC-600 before and after the reaction. The peaks located at 710.8 eV and 724.6 eV correspond to $2p_{3/2}$ and $2p_{1/2}$ of Fe^{2+}, and the peaks at 714.4 eV and 727.4 eV are assigned to the $2p_{3/2}$ and $2p_{1/2}$ of Fe^{3+}, indicating the existence of Fe^{2+} and Fe^{3+} in FSC-600 (Wu *et al.* 2015). In addition, the satellite peak of Fe(III) was observed at 719.62 eV in FSC-600 (Grosvenor *et al.* 2004), further proving the existence of Fe_2O_3 in FSC-600. According to the XRD characterization, Fe_2O_3 and Fe^0 coexisted in FSC-600. However, because of the limited penetration depth of XPS (Lin & Chen 2017), no Fe^0 signal appeared in FSC-600.

3.2. Factors influencing the degradation of phenol

3.2.1. pH value

The pH value plays an important role in Fenton reaction and degradation of organic contaminants, so the degradation performance of materials obtained at different calcination temperatures were evaluated under different pH values. As shown in Figure 4, FSC-X00 showed good degradation performance when the pH value was 3, the degradation efficiency of phenol was close to 100% after 5 min except for FSC-900. However, phenol can still be mostly degraded after 15 min by FSC-900. When the pH value was 4, FSC-X00 material also showed relatively good degradation efficiency and reached 100% after 15 min. However, as the pH value increased, the phenol degradation efficiency of FSC-X00 decreased. The degradation efficiency of FSC-X00 in 40 min decreased from 100% to 40% when the pH value was 6. When the pH value rose to 8, the degradation efficiency decreased more significantly and the degradation efficiency of FSC-X00 decreased to about 15%. This suggests that acidic solutions are more favorable for the degradation of phenol by FSC-X00-H_2O_2 system. Possible reasons include: (1)

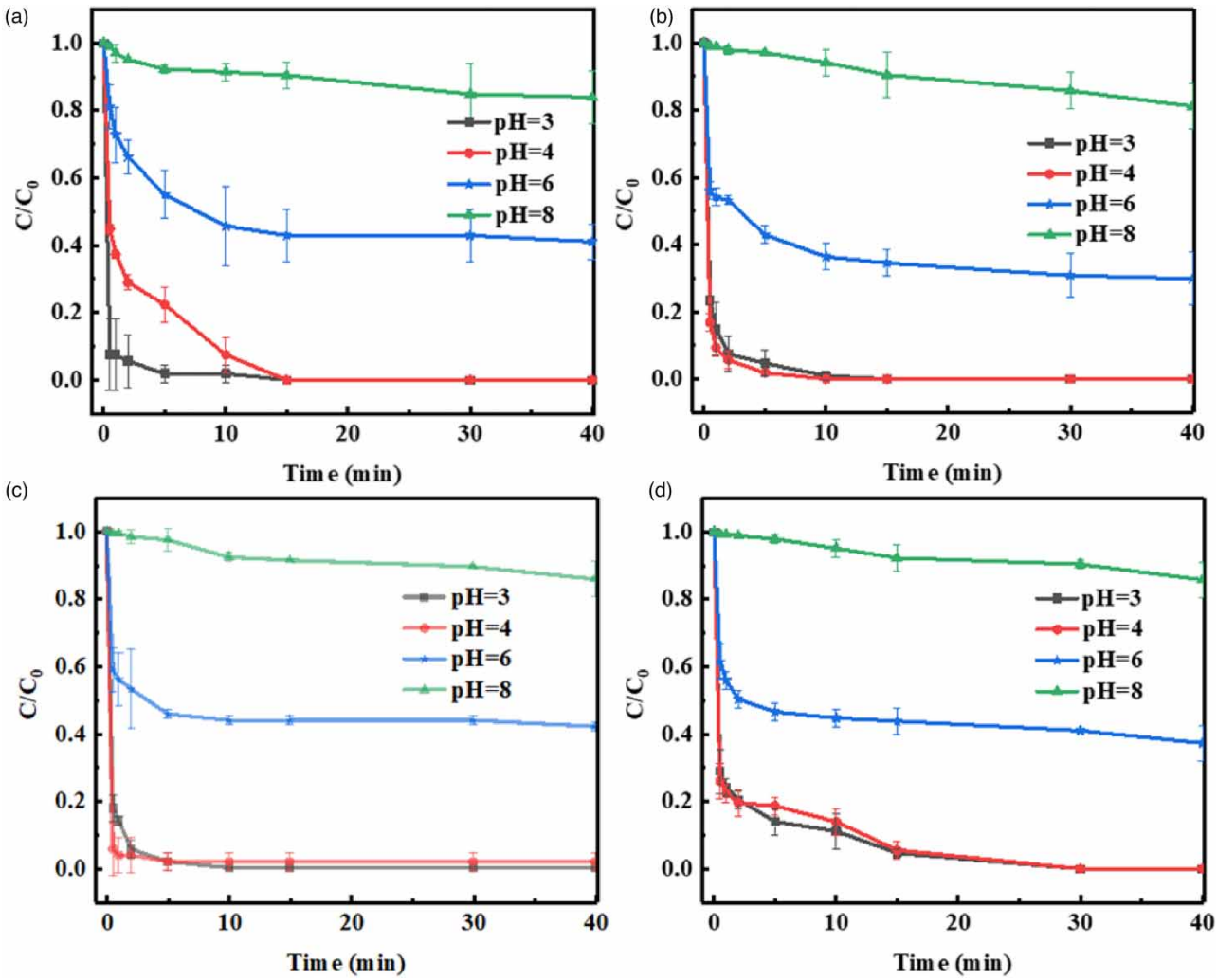

Figure 4 | The concentration variation of phenol with time at different pH value (a) FSC-600, (b) FSC-700, (c) FSC-800, and (d) FSC-900. Reaction conditions: [Phenol] = 20 mg/L, [Catalyst] = 0.4 g/L, [H_2O_2] = 4 mmol/L, T = 25 °C.

When the solution is acidic, Fe^0 can easily enter the solution to form Fe^{2+}, thus promoting H_2O_2 to produce •OH; (2) •OH has a higher reduction potential than other free radicals under acidic conditions (Mao *et al.* 2019; Fang *et al.* 2021); (3) Under acidic conditions, it is easier for Fe^{2+} to form $Fe(OH)_3$; (4) Excess OH^- will react with H_2O_2 to generate O_2 under alkaline conditions, reducing the degradation efficiency (Dong *et al.* 2016). Figure 4 shows that the degradation efficiency of the samples obtained at different calcination temperatures did not differ significantly when the pH value was 3 or 4, so a pH value of 3 was selected for the following experiments. In addition, from the perspective of energy consumption, FSC-600 was selected as the subsequent experimental material.

3.2.2. Effect of H_2O_2 and catalyst dosages

To obtain the best experimental parameters, the dosage of H_2O_2 and catalyst were screened respectively. As shown in Figure 5(a), the degradation efficiency in 40 min was about 90% when the H_2O_2 concentration was 2 mmol/L. It may be that the H_2O_2 concentration was insufficient and the •OH generated failed to complete the degradation of all phenol. The degradation efficiency was significantly enhanced when the H_2O_2 concentration was increased from 2 mmol/L (70%) to 4 mmol/L and 8 mmol/L (nearly 100%) in 5 min. However, the degradation efficiency had decreased by 10% in first 5 min when the H_2O_2 concentration reached 20 mmol/L. This may be due to the production of excessive •OH reacting with H_2O_2 to produce weak oxidizing peroxy radicals (Deng *et al.* 2018), causing degradation efficiency to decrease at the beginning ($\bullet OH + H_2O_2 \rightarrow HO_2\bullet + H_2O$). Therefore, excessive H_2O_2 may reduce the utilization rate of •OH, thereby impacting

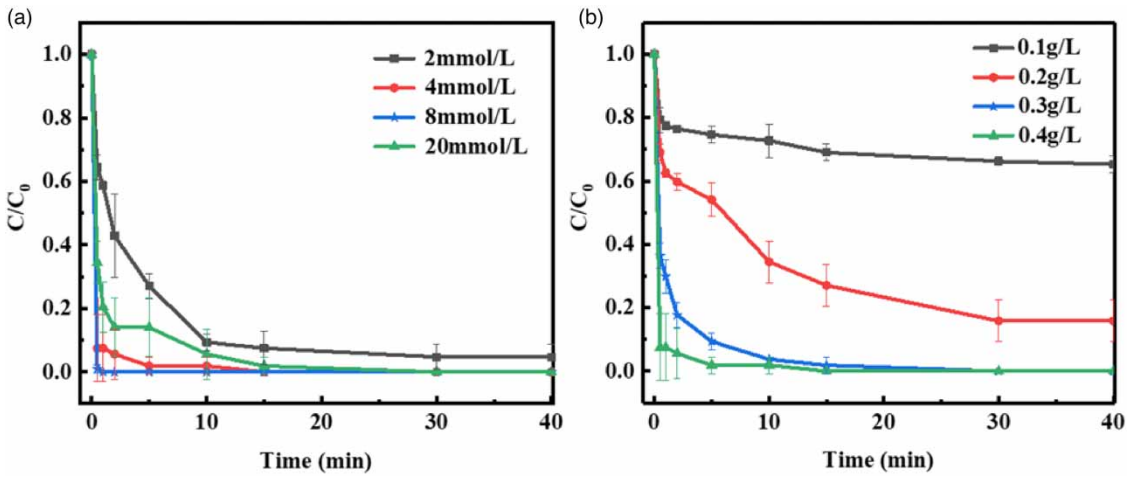

Figure 5 | Effects of (a) H_2O_2 dosage and (b) FSC-600 dosage on degradation efficiency of phenol. Reaction conditions: [Phenol] = 20 mg/L, T = 25 °C, pH = 3.

the degradation efficiency of phenol. Considering that the effect of H_2O_2 concentration is similar between 4 mmol/L and 8 mmol/L, 4 mmol/L was chosen to conduct the subsequent experiments.

From Figure 5(b), it is not difficult to find that only 30% of phenol was degraded within 40 min when the dosage was 0.1 g/L. The degradation efficiency of phenol increased from 30% to 80% (40 min) and 100% (15 min) when FSC-600 were 0.2 g/L and 0.3 g/L, respectively. The degradation efficiency could reach nearly 100% in 5 min with the dosage of FSC-600 raised up to 0.4 g/L. Therefore, 0.4 g/L was selected as the most suitable dosage.

The degradation efficiency of FSC-600-H_2O_2 systems is shown in Figure 6(a) with the BC, BC-H_2O_2, H_2O_2, and FSC-600 as control. When H_2O_2 was used alone, less than 1% of phenol was degraded within 40 min, which indicated it had almost no effect on phenol degradation. 10% of phenol was degraded by BC, BC-H_2O_2 within 40 min, which suggested that BC had no obvious activation effect on H_2O_2. When FSC-600 was used without H_2O_2, the removal efficiency of phenol was only 20%, which may come from the adsorption. However, phenol was almost completely degraded in FSC-600-H_2O_2 system within 5 min, which indicated that FSC-600 had an obvious activation effect on H_2O_2. The pseudo-first-order kinetics model was used to fit the kinetic process (Bhattacharya & Mazumder 2020; Duan *et al.* 2021). As shown in Figure S3, with the increase of phenol concentration, the degradation efficiency gradually decreased and the data fit well with pseudo-first-order kinetics model. Therefore, we believe that the degradation reaction is still dominated by kinetic control. Obviously, the k value for

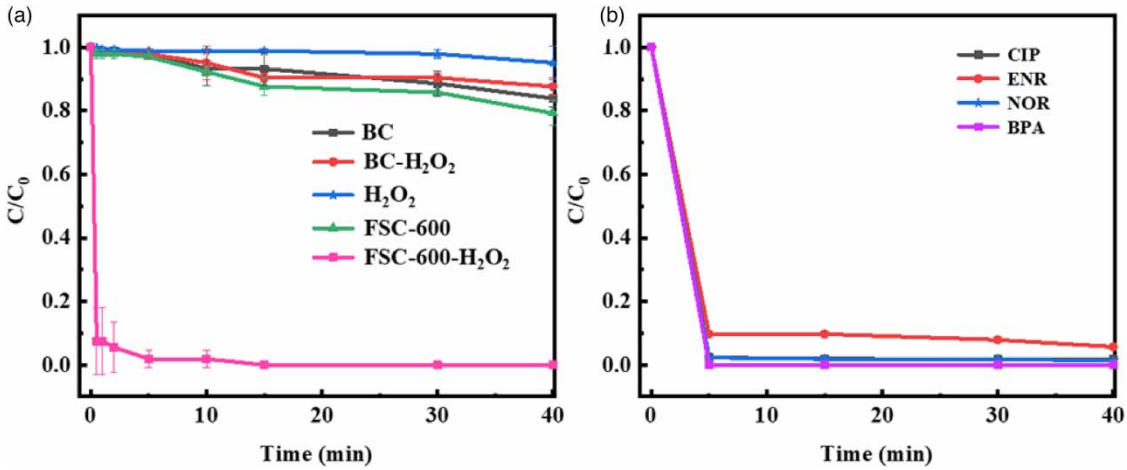

Figure 6 | (a) The degradation efficiencies for phenol in different systems; (b) The degradation efficiencies for CIP, NOR, BPA and ENR. Reaction conditions: [Phenol, CIP, NOR, ENR, BPA] = 20 mg/L, [H_2O_2] = 4 mmol/L, [Catalyst] = 0.4 g/L, T = 25 °C, pH = 3.

50 mg/L phenol was the highest, showing that the FSC-600-H_2O_2 system has an quick kinetic process for the phenol with low concentrations. In addition, Figure 6(b) shows the degradation efficiency of FSC-600-H_2O_2 system for different kinds of organic compounds. FSC-600-H_2O_2 system also shows a good degradation efficiency on CIP, BPA and NOR and the degradation efficiency can reach 100% within 5 min. The degradation efficiency of ENR was slightly worse than that of the BPA, CIP and NOR, but can still reach 95% within 5 min. When the time was extended to 40 min, the degradation efficiency was close to 97%. This shows that FSC-600 is an excellent H_2O_2 activator, and has a strong degradation effect on a variety of new pollutants within a short time period.

For advanced oxidation technology, whether organic pollutants are completely degraded into inorganic carbon is also an important indicator for evaluating performance. Hence, the total organic carbon analyzer (TOC) and three-dimensional fluorescence analyzer were used to evaluate the degree of degradation by the FSC-600-H_2O_2 system. As shown in Figure S4, about 80% of the organic carbon was converted into inorganic carbon within 30 min, and the equilibrium was reached in 60 min (about 85%). Figure 7 shows the EEM diagrams of the reaction solution at 0 and 30 min. The fluorescence center of the initial solution is in area I (Ex = 270–350 nm/Em = 240–280 nm), which corresponds to the aromatic protein in phenol. After reacting for 30 min, the fluorescence intensity weakened and the fluorescence center shifted to area II, indicating that most of the phenol was gradually decomposed into small molecular substances within 30 min. As shown in Figure S5, phenol, succinic acid, and oxalic acid were found during phenol degradation from the initial 5 to 30 min, but phenol was completely degraded after 30 min. It is well-known that •OH can attack the benzene ring by electrophilic addition reaction. Therefore, the degradation pathways of phenol were speculated. Firstly, the benzene ring was attacked to form succinic acid and then the structure was further converted into chain-like molecules of intermediates, such as oxalic acid, by oxidizing species. Finally, chain-like molecules of intermediates were mineralized into CO_2 and H_2O•. At present, the mineralization effect of iron-based materials on organic pollutants is about 70–80%, and the mineralization time is longer than that of our work (Table 1), which shows that the FSC-600 is a promising heterogeneous Fenton catalyst for degrading organic pollution within a short timeframe.

3.2.3. The effect of competing ions on degradation efficiency

To study the availability of the FSC-600-H_2O_2 system in real wastewaters, we simulated real waters by introducing natural organic matter (fulvic acid, FA) or inorganic ions (Na_2SO_4) into the phenol solution. Figure 8(a) shows the degradation efficiency of phenol in the FSC-600-H_2O_2 system under different concentrations of FA. First, when the concentration of FA was 10 mg/L, the degradation efficiency was close to 100% within 5 min. In other words, the degradation efficiency was almost unaffected. However, when the concentration of FA was 20 mg/L, the degradation efficiency reduced by about 10% in the

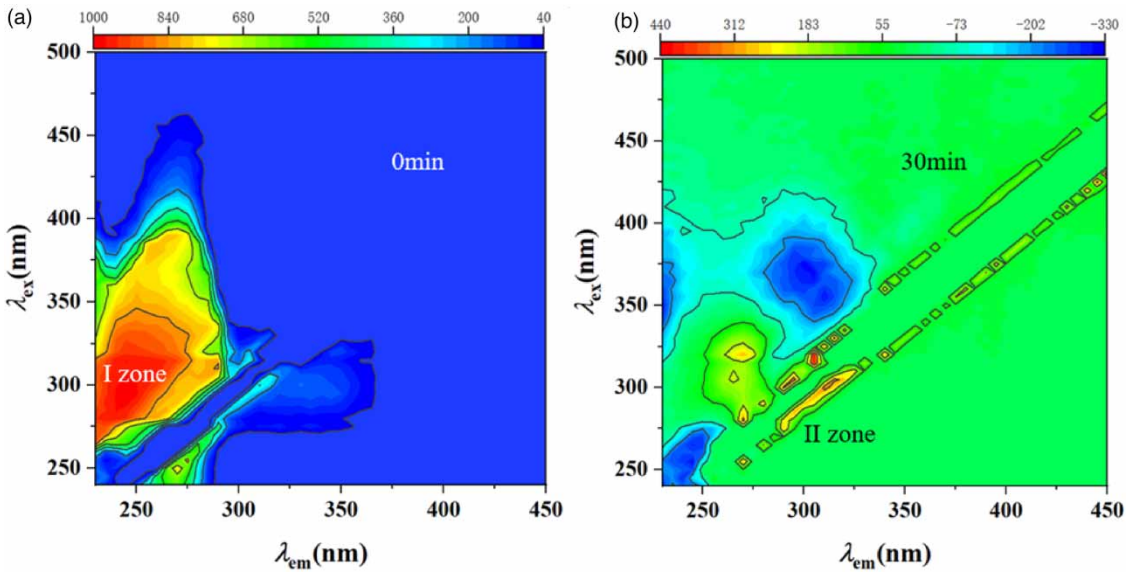

Figure 7 | The EEM of FSC-600-H_2O_2 systems (a) initial phenol solution; (b) phenol solution reaction after 30 min. Reaction conditions: [Phenol] = 20 mg/L, [H_2O_2] = 4 mmol/L, [Catalyst] = 0.4 g/L, T = 25 °C, pH = 3.

Table 1 | The degradation efficiency of organic pollutants by iron-based materials and FSC-600-H_2O_2

Materials	Pollutants (mg/L)	Reaction conditions	Degradation Time (min)	TOC removal rate	References
$FeO@Fe_2O_3$	AGB (200)	CY = 0.1 g/L $H_2O_2 = 10^{-3}$ mol/L pH = 3.8	20	72% (200 min)	Hou *et al.* (2016)
nZVI@US	4CP (100)	CY = 585 mg/L H_2O_2 = 160 mmol/L pH = 7	60	76% (60 min)	Huang *et al.* (2014)
Fe_3O_4@US	BPA (10)	CY = 0.2 g/L PMS = 0.1 g/L pH = 6	30	45% (480 min)	Zhao *et al.* (2021)
Fe@ Fe_2O_3	AOG (100)	CY = 100 mg/L H_2O_2 = 109 mmol/L pH = 7	25	85% (24 h)	Wang *et al.* (2018)
Fe@ Fe_2O_3	RhB (20)	CY = $5*10^{-5}$ mol/L $H_2O_2 = 8*10^{-5}$ mol/L pH = 4.3	30	80% (36 h)	Shi *et al.* (2014)
Fe@Mn	BPA (20)	CY = 0.5 g/L H_2O_2 = 160 mmol/L pH = 4	25	72% (180 min)	Ghanbari & Moradi (2017)
Co@Mn	Phenol (25)	CY = 0.1 g/L PMS = 1 mmol/L pH = 7	40	70% (90 min)	Zhao *et al.* (2017)
Mn@BC	Phenol (50)	CY = 1 g/L PMS = 240 mmol/L pH = 7	90	90% (90 min)	Wang *et al.* (2021a)
FSC-600	Phenol (20)	CY = 0.4 g/L H_2O_2 = 4 mmol/L pH = 3	5	80% (30 min)	This work

(Note: US = Ultrasound; CY = Catalyst; AGB = Argazol blue; 4CP = 4-chlorophenol; AOG = Acid Orange; RhB = Rhodamine B).

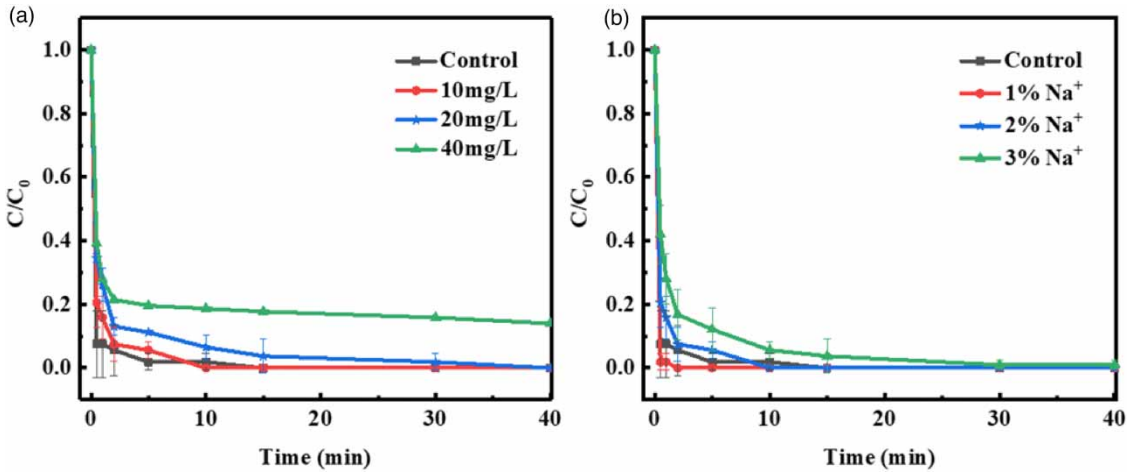

Figure 8 | Time profiles of the phenol degradation in the FSC-600-H_2O_2-system in the existence of (a) FA; (b) Na_2SO_4. Reaction conditions: [Phenol] = 20 mg/L, [Catalyst] = 0.4 g/L, [H_2O_2] = 4 mmol/L, T = 25 °C, pH = 3.

first 15 min, and it could still be basically degraded after 40 min. When the concentration of FA rose to 40 mg/L, the degradation efficiency decreased by about 20% within 40 min. The decrease may be due to the following reasons: (1) The active site was occupied by FA molecules (Mady *et al.* 2019), which lowered the adsorption of phenol; (2) Part of •OH degraded FA instead of phenol. Although the degradation efficiency decreases with the increase of FA concentration, FSC-600 can still

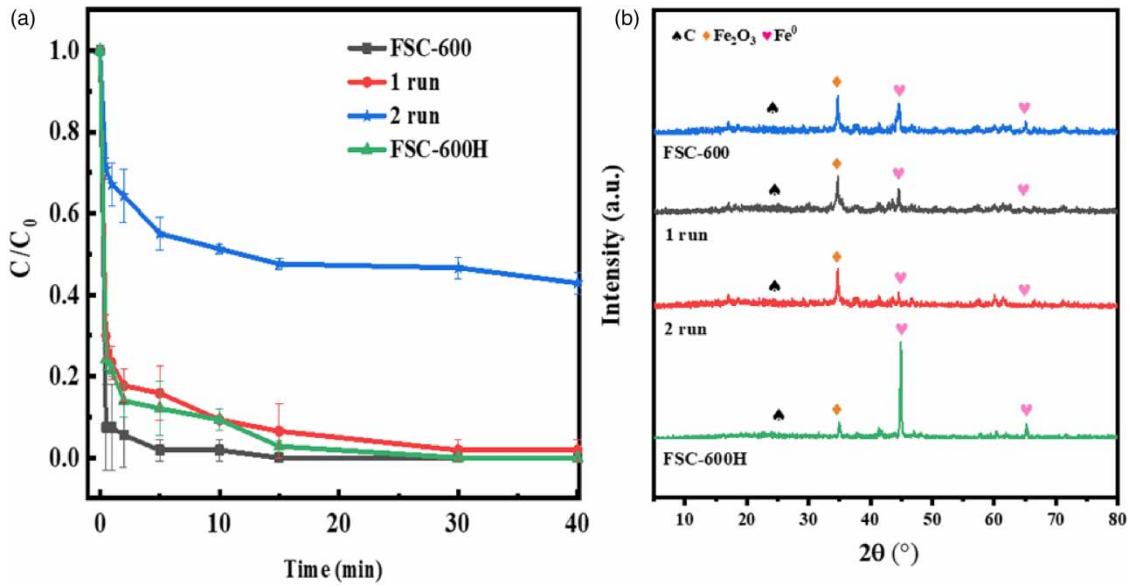

Figure 9 | (a) Reusability of FSC-600 for the degradation of phenol at pH 3; (b) XRD pattern of different samples. Reaction conditions: [Phenol] = 20 mg/L, [Catalyst] = 0.4 g/L, [H_2O_2] = 4 mmol/L, T = 25 °C.

degrade most of phenol in a short time. In addition, we investigated the degradation efficiency in the presence of inorganic salt. Figure 8(b) shows that when the Na^+ concentration was 1–2%, the FSC-600-H_2O_2 system can degrade nearly 100% of phenol within 5 min. However, the degradation efficiency decreased by about 10% within 5 min and it can still attain nearly 100% within 15 min when Na^+ concentration was 3%. Interestingly, the degradation efficiency appeared to vary mildly in Min River and Seawater (Figure S6). Therefore, the competition experiments indicate that FSC-600-H_2O_2-system may be promising not only in real water bodies but also in the domain of biphasic media (Madriz *et al.* 2011).

3.3. The cycle stability of the catalyst

The cycle stability of the catalyst is an important indicator for evaluating whether it can be applied in practice. Therefore, cycle stability experiments were carried out using FSC-600. As indicated in Figure 9(a), when the first recycled FSC-600 was used to conduct degradation experiments, the degradation efficiency decreased from 100% to about 90% within 40 min. However, the degradation efficiency was only about 60% in the second run. To understand why degradation efficiency decreased, a phase analysis of the recycled FSC-600 was conducted. As shown in Figure 9(b), the diffraction peaks of Fe^0 for the recycled FSC-600 greatly decreased after the experiment, indicating that Fe^0 was gradually consumed during the experiments. However, the diffraction peak of Fe_2O_3 still exists after two rounds of experiments. Therefore, the FSC-600 was reactivated by high-temperature calcination after two rounds of experiments (named as FSC-600H). As shown in Figure 9, the FSC-600H has a strong Fe^0 diffraction peak and its degraded efficiency towards phenol reached nearly 100% within 15 min. This means that FSC-600 can be activated for secondary use by simple calcination.

3.4. Degradation mechanism

To observe the kinds of free radicals in the FSC-600-H_2O_2 system, benzoic acid fluorescence spectrophotometry was used to observe the presence or absence of •OH in the system (Wang *et al.* 2021b). Figure 10(a) shows the variation of the fluorescence peak intensity at 405 nm for FSC-600-H_2O_2 system with different doses of tert-butanol (TBA). As indicated in Figure 10(a), the intensity of fluorescence peak at 405 nm was strong without TBA, indicating a large amount of •OH in the system, and the degradation efficiency of phenol was close to 100% at this time (Figure 10(b)). To further prove the existence of •OH, we performed EPR detection on FSC-600 and Fe_2O_3 by the DMPO-OH method. Figure 10(c) shows that both FSC-600 and Fe_2O_3 had a four-fold peak with intensity ratio of 1 : 2 : 2 : 1, which can be attributed to the characteristic peak of DMPO-OH. The intensity of DMPO-OH for FSC-600 was much stronger than that of Fe_2O_3, indicating that FSC-600 can effectively activate H_2O_2 to generate •OH. Next, when the dosage of TBA reached 30 mmol/L, the fluorescence intensity at 405 nm basically disappeared, and the degradation efficiency at this time was less than 20%, indicating that the •OH is main

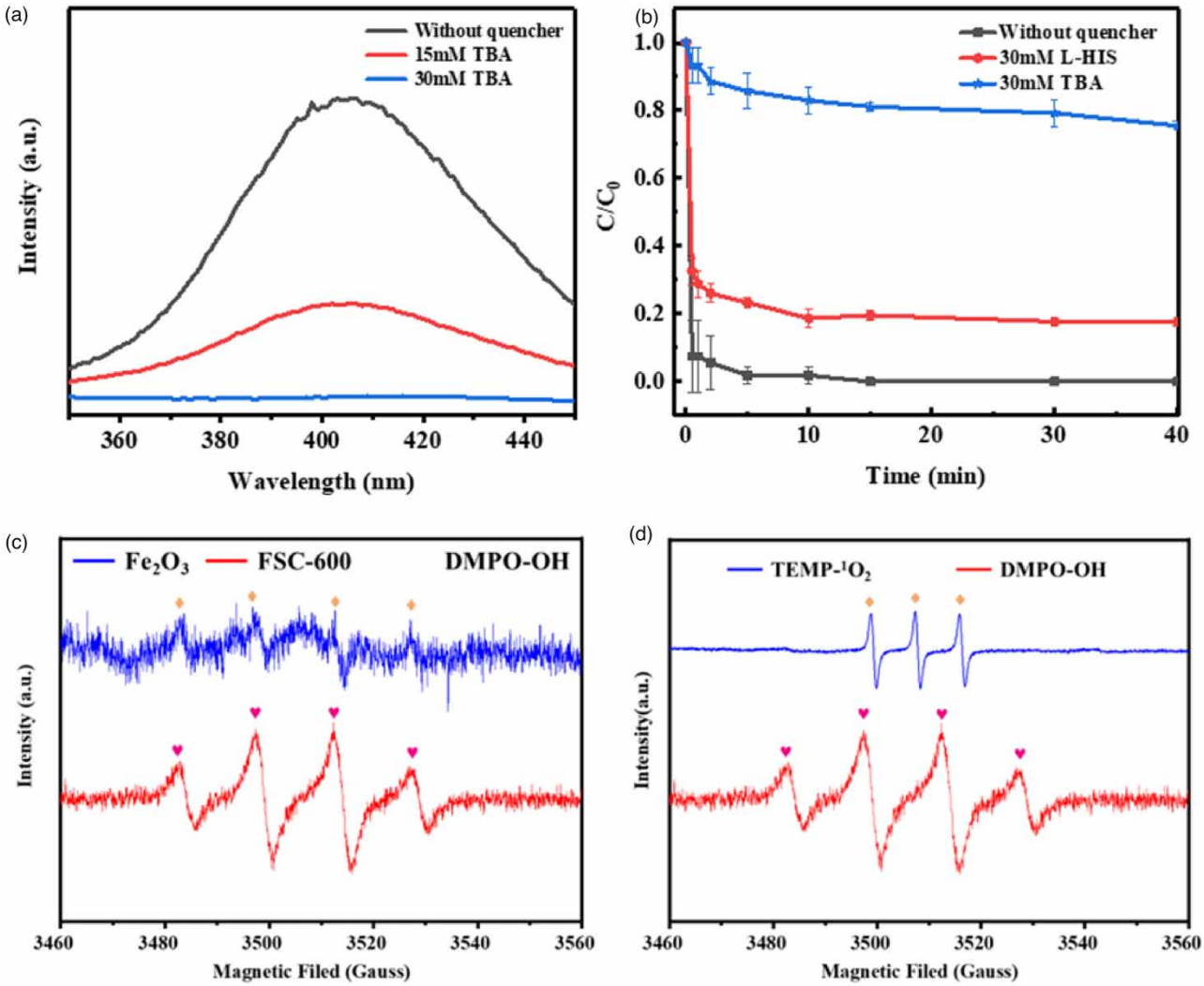

Figure 10 | (a) Fluorescence spectra in FSC-600-H_2O_2 system with and without quenching agent. (b) Time profiles of the phenol degradation in the FSC-600-H_2O_2-system in the existence of quenching agent; EPR spectra of (c) DMPO-OH and (d) TEMP-$^1O_2$ in FSC-600-H_2O_2 system;.

ROS species. From Figure 10(a) and 10(b), we found that degradation efficiency still maintained about 20% even if no •OH was detected. Therefore, L-histidine was used as a quencher to detect the presence of singlet oxygen. As displayed in Figure 10(b), the degradation efficiency is about 20% after adding 30 mmol/L of L-histidine, indicating that part of the singlet oxygen participated in the reaction. To seek the source of singlet oxygen, Figure S7 shows the degradation performance of the FSC-600-H_2O_2 system in air and argon atmospheres (Wei *et al.* 2021). Clearly, in an argon atmosphere, only about 80% of phenol was degraded within 40 min, which was similar to the experimental results of adding L-histidine. Therefore, we speculate that singlet oxygen may be formed by the oxygen dissolved in the solution with the aid of Fe^0 as an electron donor according to the following process (Equations (1) and (2)) (He *et al.* 2019). To further verify our speculation, we used TEMP as a particular spin-trapping agent for $^1O_2$. As shown in Figure 10(d), a signal with an intensity ratio of 1 : 1 : 1 resulting from TEMP-$^1O_2$ was observed in FSC-600- H_2O_2 system, indicating the existence of $^1O_2$.

$$O_2 + e^- \rightarrow O_2^- \quad (1)$$

$$O_2^- + \bullet OH \rightarrow {}^1O_2 + OH^- \quad (2)$$

Fe^{2+} can effectively activate H_2O_2 to produce •OH. Hence, the concentrations of Fe^{2+} and total dissolved irons were measured by a 1,10-phenanthroline method. As shown in Figure S8, the concentration of Fe^{2+} in the solution continued

to increase over time. The concentration of Fe^{3+} first rose and then decreased. The total iron ion concentration reached equilibrium after 30 min. We considered that Fe_2O_3 formed on the surface of Fe^0 caused the initial Fe^{3+} concentration over the Fe^{2+} concentration. In addition, Fe^{2+} in the solution can rapidly activate H_2O_2 to •OH (Equations (3)) because k_1 is greater than k_2, causing the concentration of Fe^{3+} to be higher than Fe^{2+} at the beginning. With ongoing reaction, Fe^{3+} was reduced to Fe^{2+} by H_2O_2 (Equations (4)) or organic intermediates.

$$Fe^{2+} + H_2O_2 + H^+ \rightarrow Fe^{3+} + H_2O + \bullet OH \quad (k_1 = 63 M^{-1}s^{-1}) \tag{3}$$

$$Fe^{3+} + H_2O_2 \rightarrow Fe^{2+} + HO_2\bullet + H^+ (k_2 = 0.02 M^{-1}s^{-1}) \tag{4}$$

4. CONCLUSIONS

In this study, FSC-X00 was prepared from tea stalks waste and used as a heterogeneous Fenton catalyst for organic pollution degradation within a short time period. The optimum conditions were FSC-600 = 0.4 g/L, pH = 3, H_2O_2 = 4 mmol/L. The degradation experiments showed that FSC-600 could degrade phenol, CIP, BPA and NOR with nearly 100% within 5 min. The competition experiments demonstrated that the FSC-600-H_2O_2-system presented superior anti-interference performance. EPR spectra analysis showed that •OH deriving from the activation of H_2O_2 by Fe^{2+} played a dominant role in the oxidation process. In addition, a part of $^1O_2$ resulting from O_2 was also involved during the degradation of phenol. Finally, FSC-600 can be recycled by annealing. This work indicates that the FSC-600-H_2O_2-system may be promising not only in real water bodies but also in the domain of biphasic media, and provides a reference scheme for using organic solid waste to prepare heterogeneous Fenton catalyst.

AUTHORS' CONTRIBUTIONS

Diwei Chen: Conceptualization, Methodology, Data Curation, Investigation, Formal analysis, Writing – Original Draft, Visualization; **Yonghao Wang**: Conceptualization, Methodology, Validation, Writing – Review & Editing, Supervision; **Zhiyan Zheng**: Resources, Investigation; **Feiji Zhang & Rufu Ke & Nan Sun**: Software; **Yongjing Wang**: Funding acquisition

ACKNOWLEDGEMENTS

The authors would like to acknowledge the National Natural Science Foundation of China (No. 52000035) and the National Science Foundation of Fujian Province (No. 2020Y0016).

DATA AVAILABILITY STATEMENT

All relevant data are included in the paper or its Supplementary Information.

REFERENCES

Adekunle, A. S., Oyekunle, J. A. O., Durosinmi, L. M., Saheed, O., Ajayeoba, T. A., Akinyele, O. F., Elugoke, S. E. & Oluwafemi, O. S. 2021 Comparative photocatalytic degradation of dyes in wastewater using solar enhanced iron oxide (Fe_2O_3) nanocatalysts prepared by chemical and microwave methods. *Nano-Structures & Nano-Objects* **28**, 100804.

Bhattacharya, R. & Mazumder, D. 2020 Kinetic study on nitrification of ammonium nitrogen-enriched synthetic wastewater using activated sludge. *Water Science and Technology* **81** (1), 62–70.

Bilińska, L. & Gmurek, M. 2021 Novel trends in AOPs for textile wastewater treatment. Enhanced dye by-products removal by catalytic and synergistic actions. *Water Resources and Industry* **26**, 100160.

Chen, X., Zhuan, R. & Wang, J. 2021 Assessment of degradation characteristic and mineralization efficiency of norfloxacin by ionizing radiation combined with Fenton-like oxidation. *Journal of Hazardous Materials* **404** (Pt A), 124172.

Deng, J., Dong, H., Zhang, C., Jiang, Z., Cheng, Y., Hou, K., Zhang, L. & Fan, C. 2018 Nanoscale zero-valent iron/biochar composite as an activator for Fenton-like removal of sulfamethazine. *Separation and Purification Technology* **202**, 130–137.

Dong, H., Zeng, Y., Zeng, G., Huang, D., Liang, J., Zhao, F., He, Q., Xie, Y. & Wu, Y. 2016 EDDS-assisted reduction of Cr(VI) by nanoscale zero-valent iron. *Separation and Purification Technology* **165**, 86–91.

Dror, I., Fink, L., Weiner, L. & Berkowitz, B. 2020 Elucidating the catalytic degradation of enrofloxacin by copper oxide nanoparticles through the identification of the reactive oxygen species. *Chemosphere* **258**, 127266.

Duan, J., Ji, H., Xu, T., Pan, F., Liu, X., Liu, W. & Zhao, D. 2021 Simultaneous adsorption of uranium(VI) and 2-chlorophenol by activated carbon fiber supported/modified titanate nanotubes (TNTs/ACF): effectiveness and synergistic effects. *Chemical Engineering Journal* **406**, 126752.

Fang, Y., Yang, K., Zhang, Y., Peng, C., Robledo-Cabrera, A. & López-Valdivieso, A. 2021 A new insight into the restriction of Cr(VI) removal performance of activated carbon under neutral pH condition. *Water Science and Technology* **84** (9), 2304–2317.

Ghanbari, F. & Moradi, M. 2017 Application of peroxymonosulfate and its activation methods for degradation of environmental organic pollutants: review. *Chemical Engineering Journal* **310**, 41–62.

Grosvenor, A. P., Kobe, B. A., Biesinger, M. C. & McIntyre, N. S. 2004 Investigation of multiplet splitting of Fe 2p XPS spectra and bonding in iron compounds. *Surface and Interface Analysis* **36** (12), 1564–1574.

He, D., Niu, H., He, S., Mao, L., Cai, Y. & Liang, Y. 2019 Strengthened Fenton degradation of phenol catalyzed by core/shell Fe-Pd@C nanocomposites derived from mechanochemically synthesized Fe-Metal organic frameworks. *Water Research* **162**, 151–160.

Hou, X., Huang, X., Ai, Z., Zhao, J. & Zhang, L. 2016 Ascorbic acid/Fe@Fe_2O_3: a highly efficient combined Fenton reagent to remove organic contaminants. *Journal of Hazardous Materials* **310**, 170–178.

Huang, R., Fang, Z., Fang, X. & Tsang, E. P. 2014 Ultrasonic Fenton-like catalytic degradation of bisphenol A by ferroferric oxide Fe_3O_4 nanoparticles prepared from steel pickling waste liquor. *Journal of Colloid and Interface Science* **436** (4), 258–266.

Kilic, M. Y., Abdelraheem, W. H., He, X., Kestioglu, K. & Dionysiou, D. D. 2019 Photochemical treatment of tyrosol, a model phenolic compound present in olive mill wastewater, by hydroxyl and sulfate radical-based advanced oxidation processes (AOPs). *Journal of Hazardous Materials* **367**, 734–742.

Li, Z., Sun, Y., Yang, Y., Han, Y., Wang, T., Chen, J. & Tsang, D. C. W. 2020 Biochar-supported nanoscale zero-valent iron as an efficient catalyst for organic degradation in groundwater. *Journal of Hazardous Materials* **383**, 121240.

Liang, L., Xi, F., Tan, W., Meng, X., Hu, B. & Wang, X. 2021 Review of organic and inorganic pollutants removal by biochar and biochar-based composites. *Biochar* **3** (3), 255–281.

Lin, K. A. & Chen, B. J. 2017 Prussian blue analogue derived magnetic carbon/cobalt/iron nanocomposite as an efficient and recyclable catalyst for activation of peroxymonosulfate. *Chemosphere* **166**, 146–156.

Lin, W., Liu, X., Ding, A., Ngo, H. H., Zhang, R., Nan, J., Ma, J. & Li, G. 2022 Advanced oxidation processes (AOPs)-based sludge conditioning for enhanced sludge dewatering and micropollutants removal: a critical review. *Journal of Water Process Engineering* **45**, 102468.

Liu, Z., Zhang, F.-S. & Wu, J. 2010 Characterization and application of chars produced from pinewood pyrolysis and hydrothermal treatment. *Fuel* **89** (2), 510–514.

Madriz, L., Carrero, H., Herrera, J., Cabrera, A., Canudas, N. & Fernández, L. 2011 Photocatalytic activity of metalloporphyrin–titanium mixtures in microemulsions. *Topics in Catalysis* **54** (1), 236–243.

Mady, A. H., Baynosa, M. L., Tuma, D. & Shim, J.-J. 2019 Heterogeneous activation of peroxymonosulfate by a novel magnetic 3D γ-MnO_2@$ZnFe_2O_4$/rGO nanohybrid as a robust catalyst for phenol degradation. *Applied Catalysis B: Environmental* **244**, 946–956.

Mao, Q., Zhou, Y., Yang, Y., Zhang, J., Liang, L., Wang, H., Luo, S., Luo, L., Jeyakumar, P., Ok, Y. S. & Rizwan, M. 2019 Experimental and theoretical aspects of biochar-supported nanoscale zero-valent iron activating H_2O_2 for ciprofloxacin removal from aqueous solution. *Journal of Hazardous Materials* **380**, 120848.

Mohan, H., Ramasamy, M., Ramalingam, V., Natesan, K., Duraisamy, M., Venkatachalam, J., Shin, T. & Seralathan, K. K. 2021 Enhanced visible light-driven photocatalysis of iron-oxide/titania composite: norfloxacin degradation mechanism and toxicity study. *Journal of Hazardous Materials* **412**, 125330.

Normile, H. J., Papelis, C. & Kibbey, T. C. G. 2017 Remobilization dynamics of caffeine, ciprofloxacin, and propranolol following evaporation-Induced immobilization in porous media. *Environmental Science & Technology* **51** (11), 6082–6089.

Pan, X., Gu, Z., Chen, W. & Li, Q. 2021 Preparation of biochar and biochar composites and their application in a Fenton-like process for wastewater decontamination: a review. *Science of the Total Environment* **754**, 142104.

Qi, L., Li, L., Yin, L. & Zhang, W. 2022 Study on the properties of denitrifying carbon sources from cellulose plants and their nitrogen removal mechanisms. *Water Science and Technology* **85** (2), 719–730.

Rayaroth, M. P., Aravindakumar, C. T., Shah, N. S. & Boczkaj, G. 2021 Advanced oxidation processes (AOPs) based wastewater treatment – unexpected nitration side reactions – a serious environmental issue: a review. *Chemical Engineering Journal* **123**, 133002.

Shi, J., Ai, Z. & Zhang, L. 2014 Fe@Fe_2O_3 core-shell nanowires enhanced Fenton oxidation by accelerating the Fe(III)/Fe(II) cycles. *Water Research* **59**, 145–153.

Su, P., Zhou, M., Song, G., Du, X. & Lu, X. 2020 Efficient H_2O_2 generation and spontaneous OH conversion for in-situ phenol degradation on nitrogen-doped graphene: pyrolysis temperature regulation and catalyst regeneration mechanism. *Journal of Hazardous Materials* **397**, 122681.

Wang, L., Yang, J., Li, Y., Lv, J. & Zou, J. 2016 Removal of chlorpheniramine in a nanoscale zero-valent iron induced heterogeneous Fenton system: influencing factors and degradation intermediates. *Chemical Engineering Journal* **284**, 1058–1067.

Wang, J., Liu, C., Qi, J., Li, J., Sun, X., Shen, J., Han, W. & Wang, L. 2018 Enhanced heterogeneous Fenton-like systems based on highly dispersed Fe(0)-Fe_2O_3 nanoparticles embedded ordered mesoporous carbon composite catalyst. *Environmental Pollution* **243** (Pt B), 1068–1077.

Wang, C., Zhao, J., Chen, C. & Na, P. 2021a Catalytic activation of PS/PMS over Fe-Co bimetallic oxides for phenol oxidation under alkaline conditions. *Applied Surface Science* **562**, 150134.

Wang, L., Zhang, Y. & Qian, J. 2021b Graphene aerogel-based catalysts in Fenton-like reactions for water decontamination: a short review. *Chemical Engineering Journal Advances* **8**, 100171.

Wei, K., Liu, X., Cao, S., Cui, H., Zhang, Y. & Ai, Z. 2021 Fe_2o_3@FeB composites facilitate heterogeneous Fenton process by efficient Fe(III)/Fe(II) cycle and in-situ H_2O_2 generation. *Chemical Engineering Journal Advances* **8**, 100165.

Wu, H., Wu, G. & Wang, L. 2015 Peculiar porous α-Fe_2O_3, γ-Fe_2O_3 and Fe_3O_4 nanospheres: facile synthesis and electromagnetic properties. *Powder Technology* **269**, 443–451.

Xiao, Y., Lyu, H., Tang, J., Wang, K. & Sun, H. 2020 Effects of ball milling on the photochemistry of biochar: enrofloxacin degradation and possible mechanisms. *Chemical Engineering Journal* **384**, 123311.

Xiaoliang, F., Cao, Q., Meng, F., Song, B., Bai, Z., Zhao, Y., Chen, D., Zhou, Y. & Song, M. 2021 A Fenton-like system of biochar loading Fe-Al layered double hydroxides (FeAl-LDH@BC)/H_2O_2 for phenol removal. *Chemosphere* **266**, 128992.

Xu, L. & Wang, J. 2011 A heterogeneous Fenton-like system with nanoparticulate zero-valent iron for removal of 4-chloro-3-methyl phenol. *Journal of Hazardous Materials* **186** (1), 256–264.

Xu, R., Ren, H., Chi, T., Zheng, Y., Xie, Y., Tian, J. & Chen, L. 2022 Ozone oxidation of 2,4,6-TCP in the presence of halide ions: kinetics, degradation pathways and toxicity evaluation. *Chemosphere* **288**, 132343.

Yang, S., Qiu, X., Jin, P., Dzakpasu, M., Wang, X. C., Zhang, Q., Zhang, L., Yang, L., Ding, D., Wang, W. & Wu, K. 2018 MOF-templated synthesis of $cofe_2o_4$ nanocrystals and its coupling with peroxymonosulfate for degradation of bisphenol A. *Chemical Engineering Journal* **353**, 329–339.

Yang, Y., Xu, D., Zhang, B., Xue, Z. & Mu, T. 2021 Substrate molecule adsorption energy: an activity descriptor for electrochemical oxidation of 5-Hydroxymethylfurfural (HMF). *Chemical Engineering Journal* **18**, 133842.

Ye, S., Zeng, G., Tan, X., Wu, H., Liang, J., Song, B., Tang, N., Zhang, P., Yang, Y., Chen, Q. & Li, X. 2020 Nitrogen-doped biochar fiber with graphitization from Boehmeria nivea for promoted peroxymonosulfate activation and non-radical degradation pathways with enhancing electron transfer. *Applied Catalysis B: Environmental* **269**, 118850.

Yuan, P., Ma, H., Shen, B. & Ji, Z. 2022 Abatement of NO/SO_2/Hg^0 from flue gas by advanced oxidation processes (AOPs): tech-category, status quo and prospects. *Science of The Total Environment* **806**, 150958.

Zha, S., Cheng, Y., Gao, Y., Chen, Z., Megharaj, M. & Naidu, R. 2014 Nanoscale zero-valent iron as a catalyst for heterogeneous Fenton oxidation of amoxicillin. *Chemical Engineering Journal* **255**, 141–148.

Zhang, C., Li, N., Chen, D., Xu, Q., Li, H., He, J. & Lu, J. 2021 The ultrasonic-induced-piezoelectric enhanced photocatalytic performance of ZnO/CdS nanofibers for degradation of bisphenol A. *Journal of Alloys and Compounds* **885**, 160987.

Zhang, M., Zhang, K., Zhou, R. & Wang, J. 2022 Hydroxylamine enhanced activation of peroxymonosulfate by Fe(III)/Cu(II) bimetallic for high-efficiency degradation of AO7. *Water Science and Technology* **85** (7), 2038–2050.

Zhao, Z., Zhao, J. & Yang, C. 2017 Efficient removal of ciprofloxacin by peroxymonosulfate/mn_3o_4 -MnO_2 catalytic oxidation system. *Chemical Engineering Journal* **327**, 481–489.

Zhao, C., Shao, B., Yan, M., Liu, Z., Liang, Q., He, Q., Wu, T., Liu, Y., Pan, Y., Huang, J., Wang, J., Liang, J. & Tang, L. 2021 Activation of peroxymonosulfate by biochar-based catalysts and applications in the degradation of organic contaminants: a review. *Chemical Engineering Journal* **416**, 128829.

First received 29 December 2021; accepted in revised form 25 April 2022. Available online 7 May 2022